

## First X-ray polarization measurement confirms the low black-hole spin in LMC X-3

JIRÍ SVOBODA <sup>1</sup>, MICHAL DOVČIAK <sup>1</sup>, JAMES F. STEINER <sup>2</sup>, FABIO MULERI <sup>3</sup>, ADAM INGRAM <sup>4</sup>,  
ANASTASIYA YILMAZ <sup>1,5,6</sup>, NICOLE RODRIGUEZ CAVERO <sup>7</sup>, LORENZO MARRA <sup>8</sup>, JURI POUTANEN <sup>9</sup>,  
ALEXANDRA VELEDINA <sup>9,10</sup>, MEHRNOOSH RAHBARDAR MOJAVER <sup>11</sup>, STEFANO BIANCHI <sup>12</sup>, JAVIER A. GARCÍA <sup>13</sup>,  
PHILIP KAARET <sup>14</sup>, HENRIC KRAWCZYNSKI <sup>15</sup>, GIORGIO MATT <sup>17</sup>, JAKUB PODGORNÝ <sup>1,16,5</sup>,  
MARTIN C. WEISSKOPF <sup>14</sup>, FABIAN KISLAT <sup>17</sup>, PIERRE-OLIVIER PETRUCCI <sup>18</sup>, MAIMOUNA BRIGITTE <sup>1,5,6</sup>,  
MICHAL BURSA <sup>1</sup>, SERGIO FABIANI <sup>3</sup>, KUN HU <sup>7</sup>, SOHEE CHUN <sup>7</sup>, GUGLIELMO MASTROSERIO <sup>19</sup>,  
ROMANA MIKUŠINCOVÁ <sup>12</sup>, AJAY RATHEESH <sup>3</sup>, ROGER W. ROMANI <sup>20</sup>, PAOLO SOFFITTA <sup>3</sup>,  
FRANCESCO URSINI <sup>8</sup>, SILVIA ZANE <sup>21</sup>, IVÁN AGUDO <sup>22</sup>, LUCIO A. ANTONELLI <sup>23,24</sup>, MATTEO BACHETTI <sup>25</sup>,  
LUCA BALDINI <sup>26,27</sup>, WAYNE H. BAUMGARTNER <sup>14</sup>, RONALDO BELLAZZINI <sup>26</sup>, STEPHEN D. BONGIORNO <sup>14</sup>,  
RAFFAELLA BONINO <sup>28,29</sup>, ALESSANDRO BREZ <sup>26</sup>, NICCOLÒ BUCCIANTINI <sup>30,31,32</sup>, FIAMMA CAPITANO <sup>3</sup>,  
SIMONE CASTELLANO <sup>26</sup>, ELISABETTA CAVAZZUTI <sup>33</sup>, CHIEN-TING CHEN <sup>34</sup>, STEFANO CIPRINI <sup>35,24</sup>,  
ENRICO COSTA <sup>3</sup>, ALESSANDRA DE ROSA <sup>3</sup>, ETTORE DEL MONTE <sup>3</sup>, LAURA DI GESU <sup>33</sup>, NICCOLÒ DI LALLA <sup>20</sup>,  
ALESSANDRO DI MARCO <sup>3</sup>, IMMACOLATA DONNARUMMA <sup>33</sup>, VICTOR DOROSHENKO <sup>36</sup>, STEVEN R. EHLERT <sup>14</sup>,  
TERUAKI ENOTO <sup>37</sup>, YURI EVANGELISTA <sup>3</sup>, RICCARDO FERRAZZOLI <sup>3</sup>, SHUICHI GUNJI <sup>38</sup>, KIYOSHI HAYASHIDA <sup>39</sup>,  
JEREMY HEYL <sup>40</sup>, WATARU IWAKIRI <sup>41</sup>, SVETLANA G. JORSTAD <sup>42,43</sup>, VLADIMÍR KARAS <sup>1</sup>, TAKAO KITAGUCHI <sup>37</sup>,  
JEFFERY J. KOLODZIEJCZAK <sup>14</sup>, FABIO LA MONACA <sup>3</sup>, LUCA LATRONICO <sup>28</sup>, IOANNIS LIODAKIS <sup>44</sup>,  
SIMONE MALDERA <sup>28</sup>, ALBERTO MANFREDA <sup>45</sup>, FRÉDÉRIC MARIN <sup>16</sup>, ANDREA MARINUCCI <sup>33</sup>,  
ALAN P. MARSCHER <sup>42</sup>, HERMAN L. MARSHALL <sup>46</sup>, FRANCESCO MASSARO <sup>28,29</sup>, IKUYUKI MITSUSHI <sup>47</sup>,  
TSUNEFUMI MIZUNO <sup>48</sup>, MICHELA NEGRO <sup>49</sup>, CHI-YUNG NG <sup>50</sup>, STEPHEN L. O'DELL <sup>14</sup>, NICOLA OMODEI <sup>20</sup>,  
CHIARA OPPEDISANO <sup>28</sup>, ALESSANDRO PAPITTO <sup>23</sup>, GEORGE G. PAVLOV <sup>51</sup>, ABEL L. PEIRSON <sup>20</sup>,  
MATTEO PERRI <sup>24,23</sup>, MELISSA PESCE-ROLLINS <sup>26</sup>, MAURA PILIA <sup>25</sup>, ANDREA POSSENTI <sup>25</sup>,  
SIMONETTA PUCCETTI <sup>24</sup>, BRIAN D. RAMSEY <sup>14</sup>, JOHN RANKIN <sup>3</sup>, OLIVER J. ROBERTS <sup>34</sup>, CARMELO SGRÒ <sup>26</sup>,  
PATRICK SLANE <sup>2</sup>, GLORIA SPANDRE <sup>26</sup>, DOUGLAS A. SWARTZ <sup>34</sup>, TORU TAMAGAWA <sup>37</sup>, FABRIZIO TAVECCHIO <sup>52</sup>,  
ROBERTO TAVERNA <sup>53</sup>, YUZURU TAWARA <sup>47</sup>, ALLYN F. TENNANT <sup>14</sup>, NICHOLAS E. THOMAS <sup>14</sup>,  
FRANCESCO TOMBESI <sup>54,35,55</sup>, ALESSIO TROIS <sup>25</sup>, SERGEY S. TSYGANKOV <sup>9</sup>, ROBERTO TUROLLA <sup>53,21</sup>,  
JACCO VINK <sup>56</sup>, KINWAH WU <sup>21</sup> AND FEI XIE <sup>57,3</sup>

<sup>1</sup> *Astronomical Institute of the Czech Academy of Sciences, Boční II 1401/1, 14100 Praha 4, Czech Republic*

<sup>2</sup> *Center for Astrophysics, Harvard & Smithsonian, 60 Garden St, Cambridge, MA 02138, USA*

<sup>3</sup> *INAF Istituto di Astrofisica e Planetologia Spaziali, Via del Fosso del Cavaliere 100, 00133 Roma, Italy*

<sup>4</sup> *School of Mathematics, Statistics, and Physics, Newcastle University, Newcastle upon Tyne NE1 7RU, UK*

<sup>5</sup> *Astronomical Institute, Faculty of Mathematics and Physics, Charles University, V Holešovičkách 2, Prague 8, 180 00, Czech Republic*

<sup>6</sup> *Institute of Theoretical Physics, Faculty of Mathematics and Physics, Charles University, V Holešovičkách 2, CZ-180 00 Praha 8, Czech Republic*

<sup>7</sup> *Physics Department, McDonnell Center for the Space Sciences, and Center for Quantum Leaps, Washington University in St. Louis, St. Louis, MO 63130, USA*

<sup>8</sup> *Dipartimento di Matematica e Fisica, Università degli Studi Roma Tre, Via della Vasca Navale 84, 00146 Roma, Italy*

<sup>9</sup> *Department of Physics and Astronomy, 20014 University of Turku, Finland*

<sup>10</sup> *Nordita, KTH Royal Institute of Technology and Stockholm University, Hannes Alfvéns väg 12, SE-10691 Stockholm, Sweden*

<sup>11</sup> *Physics Department, Washington University in St. Louis, St. Louis, MO 63130, USA*

<sup>12</sup> *Dipartimento di Matematica e Fisica, Università degli Studi Roma Tre, Via della Vasca Navale 84, 00146 Roma, Italy*

<sup>13</sup> *California Institute of Technology, Pasadena, CA 91125, USA*

<sup>14</sup> *NASA Marshall Space Flight Center, Huntsville, AL 35812, USA*

<sup>15</sup> *Physics Department and McDonnell Center for the Space Sciences, Washington University in St. Louis, St. Louis, MO 63130, USA*

<sup>16</sup> *Université de Strasbourg, CNRS, Observatoire Astronomique de Strasbourg, UMR 7550, 67000 Strasbourg, France*

<sup>17</sup> *Department of Physics and Astronomy and Space Science Center, University of New Hampshire, Durham, NH 03824, USA*

<sup>18</sup> *Université Grenoble Alpes, CNRS, IPAG, 38000 Grenoble, France*

<sup>19</sup> *INAF-Osservatorio Astronomico di Cagliari, via della Scienza 5, I-09047 Selargius (CA), Italy*

<sup>20</sup> *Department of Physics and Kavli Institute for Particle Astrophysics and Cosmology, Stanford University, Stanford, California 94305, USA*

<sup>21</sup> *Mullard Space Science Laboratory, University College London, Holmbury St Mary, Dorking, Surrey RH5 6NT, UK*

<sup>22</sup> *Instituto de Astrofísica de Andalucía – CSIC, Glorieta de la Astronomía s/n, 18008 Granada, Spain*

- <sup>23</sup>INAF Osservatorio Astronomico di Roma, Via Frascati 33, 00040 Monte Porzio Catone (RM), Italy
- <sup>24</sup>Space Science Data Center, Agenzia Spaziale Italiana, Via del Politecnico snc, 00133 Roma, Italy
- <sup>25</sup>INAF Osservatorio Astronomico di Cagliari, Via della Scienza 5, 09047 Selargius (CA), Italy
- <sup>26</sup>Istituto Nazionale di Fisica Nucleare, Sezione di Pisa, Largo B. Pontecorvo 3, 56127 Pisa, Italy
- <sup>27</sup>Dipartimento di Fisica, Università di Pisa, Largo B. Pontecorvo 3, 56127 Pisa, Italy
- <sup>28</sup>Istituto Nazionale di Fisica Nucleare, Sezione di Torino, Via Pietro Giuria 1, 10125 Torino, Italy
- <sup>29</sup>Dipartimento di Fisica, Università degli Studi di Torino, Via Pietro Giuria 1, 10125 Torino, Italy
- <sup>30</sup>INAF Osservatorio Astrofisico di Arcetri, Largo Enrico Fermi 5, 50125 Firenze, Italy
- <sup>31</sup>Dipartimento di Fisica e Astronomia, Università degli Studi di Firenze, Via Sansone 1, 50019 Sesto Fiorentino (FI), Italy
- <sup>32</sup>Istituto Nazionale di Fisica Nucleare, Sezione di Firenze, Via Sansone 1, 50019 Sesto Fiorentino (FI), Italy
- <sup>33</sup>Agenzia Spaziale Italiana, Via del Politecnico snc, 00133 Roma, Italy
- <sup>34</sup>Science and Technology Institute, Universities Space Research Association, Huntsville, AL 35805, USA
- <sup>35</sup>Istituto Nazionale di Fisica Nucleare, Sezione di Roma “Tor Vergata”, Via della Ricerca Scientifica 1, 00133 Roma, Italy
- <sup>36</sup>Institut für Astronomie und Astrophysik, Universität Tübingen, Sand 1, 72076 Tübingen, Germany
- <sup>37</sup>RIKEN Cluster for Pioneering Research, 2-1 Hirosawa, Wako, Saitama 351-0198, Japan
- <sup>38</sup>Yamagata University, 1-4-12 Kojirakawa-machi, Yamagata-shi 990-8560, Japan
- <sup>39</sup>Osaka University, 1-1 Yamadaoka, Suita, Osaka 565-0871, Japan
- <sup>40</sup>University of British Columbia, Vancouver, BC V6T 1Z4, Canada
- <sup>41</sup>International Center for Hadron Astrophysics, Chiba University, Chiba 263-8522, Japan
- <sup>42</sup>Institute for Astrophysical Research, Boston University, 725 Commonwealth Avenue, Boston, MA 02215, USA
- <sup>43</sup>Department of Astrophysics, St. Petersburg State University, Universitetsky pr. 28, Petrodvoretz, 198504 St. Petersburg, Russia
- <sup>44</sup>Finnish Centre for Astronomy with ESO, 20014 University of Turku, Finland
- <sup>45</sup>Istituto Nazionale di Fisica Nucleare, Sezione di Napoli, Strada Comunale Cinthia, 80126 Napoli, Italy
- <sup>46</sup>MIT Kavli Institute for Astrophysics and Space Research, Massachusetts Institute of Technology, 77 Massachusetts Avenue, Cambridge, MA 02139, USA
- <sup>47</sup>Graduate School of Science, Division of Particle and Astrophysical Science, Nagoya University, Furo-cho, Chikusa-ku, Nagoya, Aichi 464-8602, Japan
- <sup>48</sup>Hiroshima Astrophysical Science Center, Hiroshima University, 1-3-1 Kagamiyama, Higashi-Hiroshima, Hiroshima 739-8526, Japan
- <sup>49</sup>Department of Physics and Astronomy, Louisiana State University, Baton Rouge, LA 70803, USA
- <sup>50</sup>Department of Physics, University of Hong Kong, Pokfulam, Hong Kong
- <sup>51</sup>Department of Astronomy and Astrophysics, Pennsylvania State University, University Park, PA 16801, USA
- <sup>52</sup>INAF Osservatorio Astronomico di Brera, via E. Bianchi 46, 23807 Merate (LC), Italy
- <sup>53</sup>Dipartimento di Fisica e Astronomia, Università degli Studi di Padova, Via Marzolo 8, 35131 Padova, Italy
- <sup>54</sup>Dipartimento di Fisica, Università degli Studi di Roma “Tor Vergata”, Via della Ricerca Scientifica 1, 00133 Roma, Italy
- <sup>55</sup>Department of Astronomy, University of Maryland, College Park, Maryland 20742, USA
- <sup>56</sup>Anton Pannekoek Institute for Astronomy & GRAPPA, University of Amsterdam, Science Park 904, 1098 XH Amsterdam, The Netherlands
- <sup>57</sup>Guangxi Key Laboratory for Relativistic Astrophysics, School of Physical Science and Technology, Guangxi University, Nanning 530004, China

## ABSTRACT

X-ray polarization is a powerful tool to investigate the geometry of accreting material around black holes, allowing independent measurements of the black hole spin and orientation of the innermost parts of the accretion disk. We perform the X-ray spectro-polarimetric analysis of an X-ray binary system in the Large Magellanic Cloud, LMC X-3, that hosts a stellar-mass black hole, known to be persistently accreting since its discovery. We report the first detection of the X-ray polarization in LMC X-3 with the Imaging X-ray Polarimetry Explorer, and find the average polarization degree of  $3.2\% \pm 0.6\%$  and a constant polarization angle  $-42^\circ \pm 6^\circ$  over the 2–8 keV range. Using accompanying spectroscopic observations by NICER, NuSTAR, and the Neil Gehrels Swift observatories, we confirm previous measurements of the black hole spin via the X-ray continuum method,  $a \approx 0.2$ . From polarization analysis only, we found consistent results with low black-hole spin, with an upper limit of  $a < 0.7$  at a 90% confidence level. A slight increase of the polarization degree with energy, similar to other black-hole X-ray binaries in the soft state, is suggested from the data but with a low statistical significance.

*Keywords:* accretion, accretion disks – black hole physics – polarization – X-rays: binaries – X-rays:  
individual: LMC X-3

## 1. INTRODUCTION

Accreting stellar-mass black hole X-ray binaries (BHXRBs) are among the brightest X-ray sources in our Galaxy. Only a few are persistent sources. Most of them are transients characterized by short, weeks to months, periods of activity and longer, years to decades, quiescent episodes (Frank et al. 2002; Zdziarski & Gierliński 2004). BHXRBs have been found to swing between different spectral states, which are distinguished by broad-band spectra and timing characteristics (Zdziarski & Gierliński 2004; Done et al. 2007; Belloni 2010). In the hard state, the spectrum has a power-law-like shape that is believed to be produced by multiple Compton (up-)scattering events of low-energy photons in a hot medium, referred to as a hot accretion flow or a corona. The soft-state spectrum resembles blackbody radiation, and is commonly attributed to the multicolor emission of the disk (Shakura & Sunyaev 1973; Novikov & Thorne 1973), which is extending down to the innermost stable circular orbit (ISCO). The shape of the spectrum is tightly related to the radius of the ISCO and, by extension, the black-hole spin. This property enables the determination of BH spins using the so-called continuum fitting method (Shafee et al. 2006; McClintock et al. 2014).

X-ray polarization offers an alternative means to probe the topology of accreting matter and these measurements have become accessible following the launch of the Imaging X-ray Polarimetry Explorer (IXPE, Weisskopf et al. 2022). The first results on the hard-state BHXRB Cyg X-1 suggest the hot medium is extended along the disc plane (Krawczynski et al. 2022), and may have a substantial outflow velocity (Poutanen et al. 2023). Another persistent source Cyg X-3 instead was found to possess an optically thick, elevated envelope resulting from super-Eddington accretion (Veledina et al. 2023).

It has been anticipated that the energy dependence of X-ray polarization degree (PD) and polarization angle (PA) in the soft-state sources could be utilized for measuring the black-hole spin (e.g., Dovčiak et al. 2008; Schnittman & Krolik 2009; Mikusincova et al. 2023). Polarization in the accretion disk (Rees 1975) can be produced by electron scattering in the upper layers of the disk (a disk atmosphere). For the case of a razor-thin semi-infinite atmosphere, the PD is a known function of the disk inclination (Chandrasekhar 1960; Sobolev 1963). Light bending, relativistic aberration and frame-

dragging effects modify the viewing angles of different parts of the accretion disk, resulting in a characteristic rotation of PA and an overall depolarization, both of which depend on the BH spin (Connors & Stark 1977; Connors et al. 1980).

Yet, the first polarization measurements of a BHXRB in the soft-state, 4U 1630–47, revealed severe problems with this standard scenario, as neither a characteristic de-polarization nor PA rotation have been observed (Ratheesh et al. 2023). On the contrary, the observed high PD exceeding 8% and its increase with energy pose significant challenges to all existing models. These models thus invariably require parameter adjustments to account for the observed values. Follow-up observation of 4U 1630–47 in the steep power-law state (when both the disk and Comptonization continuum significantly contribute to the X-ray band) emphasize the difficulties highlighted by the soft-state data (Rodríguez Cavero et al. 2023).

Other IXPE observations of BHXRBs in the soft state include LMC X-1 (Podgorny et al. 2023), 4U 1957+115 (Marra et al. in prep.), and Cyg X-1 (Dovčiak et al. (2023), Steiner et al. in prep.). LMC X-1 is a low-inclination system. As expected, it has exhibited a low PD around 1% (Podgorny et al. 2023). In addition, a significant contribution to the polarization was possibly due to a Comptonization component. A higher inclination system, 4U 1957+115, revealed a higher polarization fraction of  $PD \approx 2\%$  (Marra et al., in prep.). Overall, the polarization properties of both sources were found to be consistent with theoretical expectations given their inclinations.

The first X-ray polarization measurement of LMC X-3 is the subject of the present study. LMC X-3 is an X-ray binary located in the Large Magellanic Cloud (LMC) at the most recently estimated distance  $D = 49.59 \pm 0.09$  (statistical)  $\pm 0.54$  (systematic) kpc (Pietrzyński et al. 2019). The mass of the black hole, companion star, and the inclination of the system are constrained from optical photometric and spectroscopic observations:  $M_{\text{BH}} = 6.98 \pm 0.56 M_{\odot}$ ,  $M_{\text{star}} = 3.63 \pm 0.57 M_{\odot}$ , and  $i = 69.2^{\circ}$  (Orosz et al. 2014), where  $M_{\odot}$  is the mass of the Sun. In the X-rays, LMC X-3 was first detected by UHURU satellite (Leong et al. 1971) and has subsequently been observed by all major X-ray satellites, owing to its persistent nature. These studies revealed the source to reside primarily in the soft state (Treves et al. 1988; Ebisawa et al. 1993; Nowak et al. 2001), with only rare hard-

state occurrences (Wilms et al. 2001; Wu et al. 2001) and occasional entry into an anomalous low state characterized by a drop in X-ray flux by a few orders of magnitude (Smale & Boyd 2012; Torpin et al. 2017).

The LMC X-3’s soft-state spectrum was found to be well modeled by a multicolor disk, whose inner temperature is proportional to the fourth root of the X-ray luminosity (Gierliński & Done 2004). Given the known distance and almost persistent stay in the high/soft state, LMC X-3 has been identified as one of the most promising targets for black-hole spin measurements using the X-ray continuum fitting method. Steiner et al. (2010) analyzed a large set of RXTE observations and found a constant inner disk radius until reaching a critical luminosity, found to be around  $0.3 L_{\text{Edd}}$  (where  $L_{\text{Edd}}$  is the Eddington luminosity,  $L_{\text{Edd}} = 1.26 \times 10^{38} M/M_{\odot} \text{ erg s}^{-1}$ ). For higher luminosities, the measured value for the innermost disk radius increased, indicating a change in the structure of the accretion disk or the disk atmosphere. To account for this behavior, slim-disk models were developed (Straub et al. 2011). The slim disk is a solution with the aspect ratio  $H/R \lesssim 1$  (where  $H$  is the scale-height of the disk and  $R$  is the radius from the center). However, the apparent increase of the innermost disk radius at high luminosity remained unsolved.

The black hole spin is closely related to the innermost disk radius, assuming the accretion disk extends down to ISCO. The first spin estimates were affected by uncertainty due to the unknown mass of the black hole. More accurate spin measurements were possible only following precise determination of the black hole’s mass from optical spectroscopy (Orosz et al. 2014). The spin was measured through the X-ray continuum fitting method as  $a \approx 0.2$  (Steiner et al. 2014). The low value of the black-hole spin has been subsequently confirmed in more recent analyses (Bhuvana et al. 2022; Yilmaz et al. 2023). Yilmaz et al. (2023) reported a measured value for black-hole spin as  $a \approx 0.1$ . In their analysis, they relaxed the condition of a constant innermost radius at ISCO and showed a scatter of the inner disk radius measurements in different observations during the outbursts (see their Figure 7 and 9).

In this paper, we present the analysis of the first IXPE observations of LMC X-3, showing that the polarimetric data are in line with the low spin of the black hole, previously measured only by X-ray spectroscopy. The observations are described in Section 2. The results of the spectro-polarimetric modeling are presented in Section 3 and discussed in Section 4. Section 5 summarizes the main results of the analysis.

## 2. OBSERVATIONS

LMC X-3 was observed in July 2023 by multiple X-ray instruments. All studied observations are summarized in Table 1. Data reduction and processing are described in more detail in the following sections.

### 2.1. IXPE

LMC X-3 was observed by IXPE on 2023 July 7–8 and 12–21 (ObsID: 02006599) with a total exposure time 562 ks. IXPE detectors (Soffitta et al. 2021) can measure the Stokes parameters  $I$ ,  $Q$ , and  $U$  and they have imaging capabilities, so that the source and background regions can be spatially separated. Level 2 event files were downloaded from the HEASARC and then filtered for source and background regions using `xpselect` tool from the IXPEOBSSIM software package version 30.5 (Baldini et al. 2022). The source extraction regions were selected for each detector unit as circles with a radius of  $60''$ . The background regions were defined as annuli with an inner radius of  $180''$  and the outer radius of  $280''$ .

Polarization cubes were generated using the unweighted `pcube` algorithm (Baldini et al. 2022). We produced PD and PA in 5 energy bins and obtained significant detection in all bins but the last. We further used IXPEOBSSIM PHA1 algorithm to generate the weighted Stokes  $I$ ,  $Q$ , and  $U$  parameters with different binning in energy. For the analysis, we used 11 bins with the bin size 0.5 keV in 2–7 keV, and 1 keV for the last 7–8 keV bin, respectively, while for plotting, we used 5 bins to compare with the unweighted `pcube` results. We further generated  $Q/I$  and  $U/I$  spectra that were converted to XSPEC-employable FITS spectra with the `FTOOL flx2xsp` with unit response matrices.

### 2.2. NICER

The Neutron-Star Interior Composition Explorer (NICER) is a soft X-ray timing mission deployed on the International Space Station (ISS). NICER is composed of 52 silicon-drift detectors, sensitive from  $\sim 0.2$ –12 keV, with  $< 100$  ns timing fidelity (Gendreau et al. 2012). Each detector is paired with a single-bounce reflector optic, all mutually co-aligned on the sky. NICER carried out two observations of LMC X-3 during the IXPE campaign, on 2023 July 8 and 17, corresponding to OBSIDs 6101010117 and 6101010118, respectively. These observations were obtained after one of the detector thermal shields was damaged in May 2023, which resulted in a light leak during ISS daytime which results in optical

**Table 1.** List of observations.

Observatory	Instrument	Observation ID	Start Date	End Date	Net exposure [ks]
IXPE	GPD	02006599	2023-07-07 18:42:31	2023-07-09 13:39:07	105.2
		02006599	2023-07-12 16:55:48	2023-07-20 14:19:34	458.6
NICER	XTI	6101010117	2023-07-08 10:10:50	2023-07-08 16:34:40	2.14
		6101010118	2023-07-17 23:37:19	2023-07-17 23:40:14	0.16
NuSTAR	FPMA/FPMB	309020041002	2023-07-09 12:16:09	2023-07-09 23:51:09	27.6
		309020041004	2023-07-14 07:56:09	2023-07-15 06:31:32	28.1
		309020041006	2023-07-19 19:41:09	2023-07-21 07:16:23	29.0
Swift	XRT	00089714001	2023-07-09 19:29:38	2023-07-09 19:31:50	1.3
		00089714002	2023-07-14 02:50:08	2023-07-14 16:54:56	1.8
		00089714003	2023-07-20 01:21:15	2023-07-20 04:42:56	1.9

loading of the detectors, producing an increase in noise and potential packet losses.<sup>1</sup>

LMC X-3 could only be observed during ISS daytime, and as a result, we found it necessary to use nonstandard filtering to recover usable data. For both observations, 42 of NICER’s 52 detectors were turned on. We screened the active detectors for outlier behavior on the basis of rates of X-ray, overshoot, and undershoot events, flagging  $> 10$ - (robust)  $\sigma$  outliers from the detector ensemble. This resulted in discarding all data from between 1–7 detectors per continuous GTI interval. We obtain a useful exposure time of  $\approx 2.2$  ks and  $\approx 160$  s, for the two observations, respectively, and were initially extracted separately per continuous GTI segment. After checking their mutual consistency, we merged them together for the spectral analysis. In order to avoid contamination from low-energy noise events which are exacerbated by the light leak, we restrict our analysis to an energy range  $> 0.5$  keV. Response products were generated based on the number of active detectors, and rates were adjusted for  $\gtrsim 1\%$  detector deadtime caused primarily by optical-loading events.

Because NICER is non-imaging, the spectral background is determined via various empirical models (Remillard et al. 2022). We adopt the SCORPEON background model,<sup>2</sup> and is normalized to the number of selected detectors.

### 2.3. NuSTAR

Three accompanying observations by the NuSTAR satellite (Harrison et al. 2013) were performed at the beginning, in the middle and at the end of the IXPE observation with the total net exposure time of  $\approx 85$  ks, see more details in Table 1. NuSTAR data were reduced using the standard Data Analysis Software (NuSTARDAS).

The NuSTAR calibration files available in the CALDB database were used to calibrate the cleaned event files, produced by the `nupipeline` task. The source regions were selected as circles with a radius of  $60''$  centered on the source image, and background regions with radius  $90''$  were selected from the corner of the same quadrant in the source-free region. The source spectrum is soft and background dominates over source above 20 keV. Therefore, we limit the NuSTAR data of LMC X-3 at high energy to be below 20 keV in all spectral analysis.

### 2.4. Neil Gehrels Swift Observatory

Simultaneous to NuSTAR, the Neil Gehrels Swift Observatory (Gehrels et al. 2004) observed LMC X-3 with exposure times of 1.3 ks (ObsID: 00089714001, 2023 July 09), 1.8 ks (ObsID: 00089714002, 14 July 2023), and 1.9 ks (ObsID: 00089714003, 2023 July 20). Individual X-ray Telescope (XRT; Burrows et al. (2005)) spectra were extracted using the standard online tools provided by the UK Swift Science Data Centre (Evans et al. 2009) using a source region of  $60''$  radius centered at the source location.

### 2.5. Software tools for data analysis

We used HEASOFT<sup>3</sup> software package (Blackburn 1995), version 6.31, for the data reduction and rebinning, and XSPEC software package (Arnaud 1996), version 12.13, for the spectral analysis. We rebinned all the NICER, NuSTAR, and Swift data with the tool `ftgrouppha` and applied optimal binning (Kaastra & Bleeker 2016) together with the condition for a minimum signal-to-noise ratio to be equal to 3. For the time-averaged spectral fits, we combined observations from multiple exposures using `ADDSPEC.PY`.<sup>4</sup> Across the entire paper, the errors are quoted as 90% confidence levels if not stated otherwise.

<sup>1</sup> [https://heasarc.gsfc.nasa.gov/docs/nicer/analysis\\_threads/light-leak-overview/](https://heasarc.gsfc.nasa.gov/docs/nicer/analysis_threads/light-leak-overview/)

<sup>2</sup> [https://heasarc.gsfc.nasa.gov/docs/nicer/analysis\\_threads/scorpeon-overview/](https://heasarc.gsfc.nasa.gov/docs/nicer/analysis_threads/scorpeon-overview/)

<sup>3</sup> <https://heasarc.gsfc.nasa.gov/docs/software/lheasoft/>

<sup>4</sup> <https://github.com/JohannesBuchner/BXA>

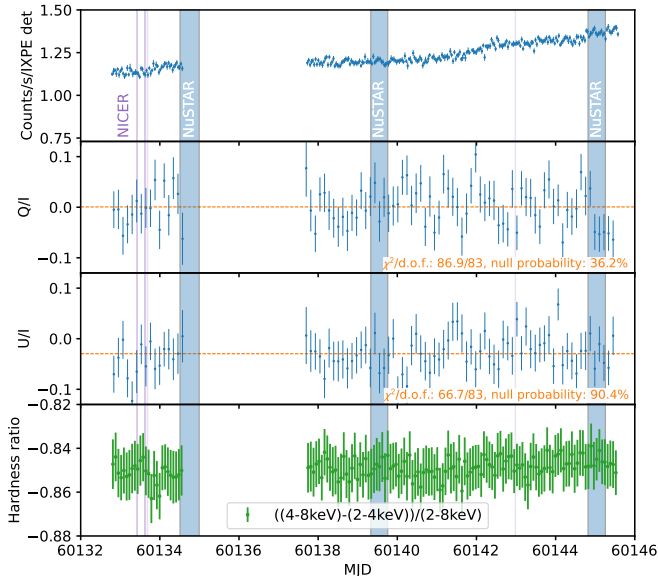


**Figure 1.** IXPE light curve: variation of the counts (*top* panel), normalized Stokes parameters  $Q/I$  (*second* panel) and  $U/I$  (*third* panel), and spectral hardness (*bottom* panel), as a function of time (in Modified Julian Date). The dates of the accompanying observations by NICER and NuSTAR are indicated as shaded regions.

### 3. RESULTS

#### 3.1. X-ray polarimetric measurements

The IXPE light curve is shown in Figure 1. LMC X-3 shows a steady continuous increase of the flux during the exposure. The count rate (averaged over all 3 GPDs) increased from about  $1.2 \text{ ct s}^{-1}$  at the beginning of the observation to  $1.5 \text{ ct s}^{-1}$  at the end of the observation. The polarization is characterized by the Stokes  $Q$  and  $U$  parameters divided by the Stokes parameter  $I$  (total number of counts). The  $Q/I$  and  $U/I$  light curves are shown in the middle panels of Figure 1. The variations observed are consistent with statistical fluctuations only, with a successful joint fit achieving  $\chi^2/\text{dof}=153.7/166$ . There is also no evidence for any significant changes in the spectral hardness, defined as the difference between counts in the hard (4–8 keV) and soft (2–4 keV) energy bands divided by the total number of counts in the 2–8 keV band, as shown in the bottom panel of Figure 1.

Using the time-integrated measurements of the Stokes parameters, we derived the PD and PA using the `xpbin` tool within the `pcube` algorithm. The average 2–8 keV PD for all three detectors is  $\text{PD} = 3.1\% \pm 0.4\%$ , and the  $\text{PA} = -45^\circ \pm 4^\circ$  with the  $1\sigma$  errors. The measurements are above the so-called minimum detectable polarization,  $\text{MDP}_{99}$ , which is the degree of polarization, for which the probability of the detection of the corresponding amplitude modulation only by chance is 1%

(Weisskopf et al. 2010). In our observation  $\text{MDP}_{99} = 1.23\%$  in 2–8 keV. The energy dependence of PD and PA is shown in Figure 2, with the data binned in 5 energy bins. Measurement of the polarization above the  $\text{MDP}_{99}$  is achieved in the entire band with the exception of the highest-energy bin (6.5–8 keV) where the  $\text{MDP}_{99}$  is higher than the actual measurement. In the 2–5 keV energy band, the PD is around 3%. An increasing trend of polarization with energy is apparent from the plot, but the measurement uncertainty gets significantly larger (see more in Section 4). The polarization angle is consistent with being a constant with only possible small deviations at higher-energy bins.

#### 3.2. X-ray spectral analysis

To properly model and interpret the polarization measurements, a robust spectral fit is first needed. For this purpose, the long IXPE observation was accompanied by several exposures with the sensitive instruments suitable for a broad-band spectroscopic analysis (see Table 1).

##### 3.2.1. Time-resolved spectroscopy with a multi-color disk blackbody and power-law model

We first analyzed the NICER, NuSTAR and Swift spectra using a simple absorbed multi-colored disk blackbody emission (Mitsuda et al. 1984) and power-law component for the Comptonization. We used `tbabs` model to account for absorption in the line-of-sight in our Galaxy (Wilms et al. 2000) and fixed the value of the hydrogen column density  $N_{\text{H}} = 4.5 \times 10^{20} \text{ cm}^{-2}$  from a full sky HI survey (HI4PI Collaboration et al. 2016). The model in XSPEC notation is `tbabs*(diskbb + powerlaw)`. We further add a cross-normalization factor to account for changes between different instruments. The disk temperature as well as the power-law photon index values were linked between different instruments and also between different exposures. Only the normalization factors of both components (disk blackbody and power law) were allowed to vary to determine if there is any spectral variability and of which component.

We found that the spectrum is dominated by the disk blackbody emission with the Comptonization component significant only for NuSTAR observations that have a coverage above 10 keV, see Figure 3. For the inner disk temperature, we obtained the value  $kT \approx 1.1 \text{ keV}$ . We get the power-law photon index of  $\Gamma \approx 2.4$ . From comparing the three Swift spectra, we see that there is no significant variability in the soft X-ray band, confirming the results suggested from the IXPE hardness ratio shown in Figure 1. The only apparent but small difference is around 1.5 keV between the first and the other observations. Similar discrepancies below 2 keV

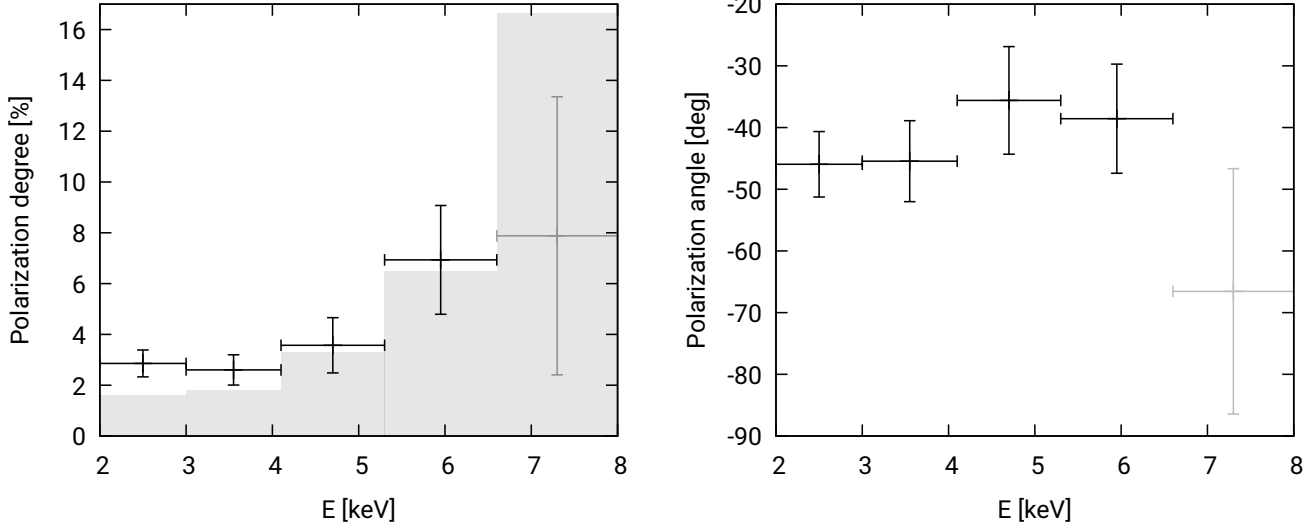


**Figure 2.** Measured PD (*left*) and PA (*right*) shown with  $1\sigma$  error bars. The shaded area in the PD-plot is an estimate of the  $MDP_{99}$ , showing the significant polarization measurements from 2 keV up to  $\approx 6.5$  keV.

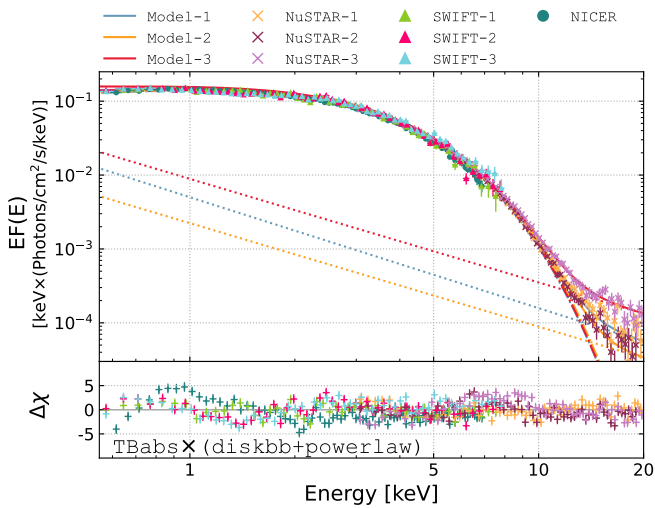


**Figure 3.** *Top:* Unfolded spectra (plot `eufspec` in XSPEC) with a joint spectral fit using the simple absorbed `diskbb+powerlaw` model employing the NICER and three Swift and NuSTAR exposures. *Bottom:* The residuals of the data from the model.

are likewise seen between Swift and NICER measurements. These residuals lead to the fit that is not formally acceptable, with a chi-square value of  $\chi^2 = 1255$  for 411 degrees of freedom ( $\chi^2_{\text{red}} \approx 3$ ).

The NuSTAR observations reveal a clear variability of the Comptonization component above  $\approx 10$  keV. The simple `diskbb + powerlaw` model allows us to estimate the fraction that is the Comptonized emission, which is less than 1% in 2–8 keV. The model decomposed in the two components is plotted in Figure 3 for the three NuSTAR observations. The strongest Comptonization com-

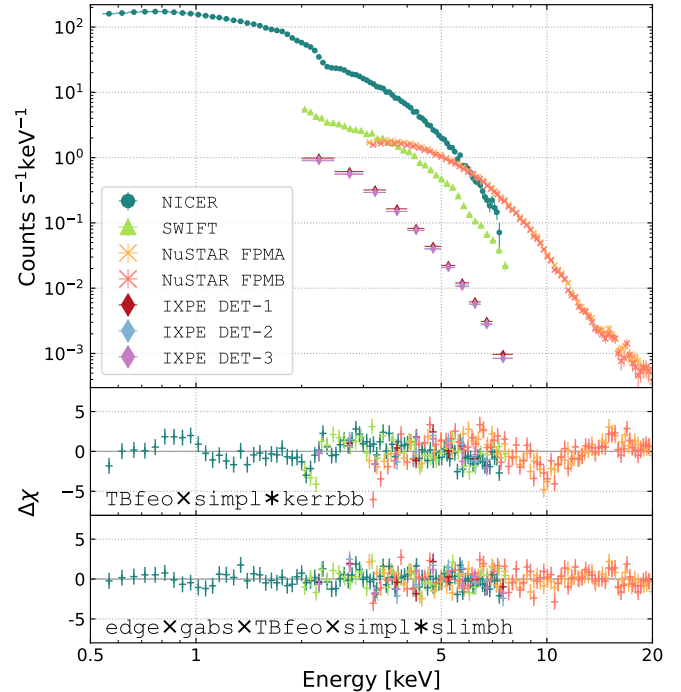


**Figure 4.** *Top:* Time-averaged NICER, NuSTAR, Swift, and IXPE data. *Middle:* The residuals of the data from the model using `tbfeo x simpl * Kerrbb`. *Bottom:* The residuals of the data from the final best-fit model.

ponent is measured in the last observation. However, it is evident from the plot that the Comptonization contributes very little to the IXPE 2–8 keV energy band, and thus we can assume that the measured polarization is related to the main component, which is the thermal emission of the accretion disk.

**Table 2.** Spectral fit parameters with the final preferred spectral model.

Component	Parameter (units)	Description	Value			
			NICER	NuSTAR	Swift	IXPE
TBfeo	$N_{\text{H}}$ ( $10^{22} \text{ cm}^{-2}$ )	H column density	$0.046 \pm 0.003$			
	O	abundance	$0.3 \pm 0.2$			
	Fe	abundance	$0.7^{+0.4}_{-0.5}$			
SLIMBH	$M_{\text{bh}}$ ( $M_{\odot}$ )	Black hole mass	6.98 (frozen)			
	$a/M$	Black hole spin	$0.19 \pm 0.02$			
	$L_{\text{Edd}}$	Luminosity	$0.40 \pm 0.01$	$0.43 \pm 0.01$	$0.41 \pm 0.02$	$0.45 \pm 0.02$
	$i$ (deg)	Inclination	69.2 (frozen)			
	$\alpha$	Viscosity	0.1 (frozen)			
	$D_{\text{bh}}$ (kpc)	Distance	49.59 (frozen)			
	hd	Color hardening	-1 (i.e. using TLUSTY)			
	$l_{\text{flag}}$	Limb-darkening	0 (frozen)			
	$v_{\text{flag}}$	Self-irradiation	0 (frozen)			
	norm	normalization	1 (frozen)			
SIMPL	$\Gamma$	Photon index	$2.7 \pm 0.3$			
	FracSctr	scattered fraction	$0.012^{+0.001}_{-0.002}$			
$\chi^2 / \text{dof}$			317/265 $\approx$ 1.2			

**Note:** The final model in the XSPEC notation is `constant*edge*gabs*tbfeo*simpl*slimbh`. Model parameters for cross-calibration and instrumental features are summarized in Table 3.**Table 3.** Modeling cross-calibration and instrumental features in the final spectral fit.

Component	Parameter	NICER	NuSTAR		Swift	IXPE		
			FPMA	FPMB		GPD 1	GPD 2	GPD 3
CONSTANT		1 (frozen)	$1.18 \pm 0.03$	$1.16 \pm 0.03$	$1.23 \pm 0.07$	$0.86 \pm 0.02$	$0.85 \pm 0.02$	$0.80 \pm 0.02$
GABS	$E$ (keV)	$2.07 \pm 0.04$	$9.9 \pm 0.1$		$2.14 \pm 0.04$	-		
	$\sigma$ (keV)	$0.08^{+0.02, \text{pegged}}_{-0.06}$	0.1 (pegged)		$0.03 \pm 0.03$	-		
EDGE	$E$ (keV)	$2.35 \pm 0.05$	-		-	-		
	$\tau$ (keV)	$0.02 \pm 0.02$	-		-	-		
GAIN	slope	-	-		-	$0.989 \pm 0.005$	$0.990 \pm 0.006$	$0.988 \pm 0.005$
	offset (keV)	-	-		-	$-0.04 \pm 0.02$	$-0.06 \pm 0.03$	$-0.05 \pm 0.02$

### 3.2.2. Spectral analysis with relativistic models for the accretion disk emission

Owing to the detection of little spectral variability, we further use merged Swift and NuSTAR spectra. There are known calibration uncertainties with the IXPE spectra, and we therefore applied the `gain` model to fit the offset slope and intercept for IXPE. We further performed a spectral analysis of 7 data sets (1 NICER, 2 NuSTAR detectors FPMA and FPMB, 1 Swift and 3 detectors of IXPE) with a cross-calibration constant fixed to 1 for NICER and allowed to vary between 0.8 and 1.2 for the other detectors. Because of the discrepancies between Swift spectra below 2 keV, we limit the merged Swift data to the 2–8 keV energy band, and use only NICER data below 2 keV. Figure 4 shows the time-averaged spectra of different detectors in the first (top) panel.

We first employed a relativistic accretion disk model `kerrbb` (Li et al. 2005) convolved with a non-relativistic

Comptonization model `simpl` (Steiner et al. 2009; Sunyaev & Titarchuk 1980), allowing for both up- and down-scattering. For absorption, we employed the `tbfeo` model allowing for different oxygen and iron abundances. Because the LMC is a low-metallicity environment, we let the abundances to be in the interval 0.25–1. The fit converged to  $N_{\text{H}} \approx 0.03 \times 10^{22} \text{ cm}^{-2}$  with the oxygen and iron abundances being pegged at their low-value limits at 0.25. We note that since the column density is lower than the column density expected in the line-of-sight in our Galaxy, the low oxygen and iron abundances may be an artifact of calibration uncertainties in the 0.5–1 keV band for NICER and/or due to variations of the absorption column within our Galaxy. No evidence for local absorption is consistent with LMC X-3’s location at a large distance from the center of the LMC, away from any gaseous nebulae.

With the `tbfeo*kerrbb*simpl` model, we obtained the dimensionless black hole spin  $a = 0.20 \pm 0.02$ , accretion rate  $\dot{M} \approx (4.5 - 5.6) \times 10^{18} \text{ g s}^{-1}$ , and the photon

index pegged at  $\Gamma = 2.0$ , which was the lowest allowed value. We allowed the hardening factor of the `kerrbb` model to vary and we obtained  $h_d \approx 1.7$  for NuSTAR and  $h_d \approx 1.9$  for NICER. The fit was formally not acceptable with  $\chi^2/\nu = 687/274 \approx 2.5$ , mainly due to discrepancies between NICER and NuSTAR data, whose residuals had opposite slopes in the overlapping energy band (see the second panel of Figure 4 at 3–8 keV energy band).

The lowest measured accretion rate  $4.5 \times 10^{18} \text{ g s}^{-1}$  corresponds to the luminosity  $L = \eta \dot{M} c^2 \approx 0.3 L_{\text{Edd}}$ , where  $\eta$  is the accretion efficiency  $\eta \approx 0.065$  (for  $a = 0.2$ ). At such a luminosity, LMC X-3 might deviate from the standard thin disk model, and a slim disk scenario was proposed to take place at the high-luminosity regime (Straub et al. 2011).

Therefore, we replaced the `kerrbb` model with the `slimbb` model (Sądowski et al. 2011; Straub et al. 2011), and we obtained a significantly better fit with  $\chi^2/\nu = 414/277 \approx 1.5$ . The `slimbb` model improved the consistency of the data residuals between NICER and NuSTAR. The only residuals were now narrow features around 2 keV and 2.4 keV for NICER and 10 keV for NuSTAR, which are visible in the second panel of Figure 4. Similar residuals were reported in some previous analyses and attributed to calibration uncertainties, see, e.g., Wang et al. (2021) for NICER and Podgorny et al. (2023) for NuSTAR. For our final model, we account for the 2 and 10 keV features with narrow Gaussian absorption lines and the 2.4 keV feature with a ‘smear-edge’ component. The goodness of the final fit is  $\chi^2/\nu = 319/266 \approx 1.2$ , which without IXPE data reduces to  $\chi^2/\nu = 259/243 \approx 1.06$ , indicating that the remaining residuals might be due to cross-calibration discrepancies. The residuals from the best-fit model are shown in the third panel of Figure 4.

The values of the best-fit model are summarized in Table 2. The spin value is consistent with the measurements using the `kerrbb` model,  $a \approx 0.20 \pm 0.02$ . The spectral hardening in the `slimbb` model is not a free parameter, but is instead calculated using the vertical structure computed using the TLUSTY code (Hubeny & Lanz 1995). The estimated luminosity is in the range  $L = 0.40\text{--}0.45 L_{\text{Edd}}$  depending on which detector is considered (the slightly higher value for IXPE can be, however, affected by the fitted cross-calibration constants lower than 1). The parameters of the Comptonization model `simpl` were constrained well only from the NuSTAR spectra and therefore, we linked the values between the different detectors. The photon index is  $\Gamma = 2.7 \pm 0.3$  and scattering fraction is  $0.012^{+0.001}_{-0.002}$ . Similarly, absorption was best constrained from the NICER data and we

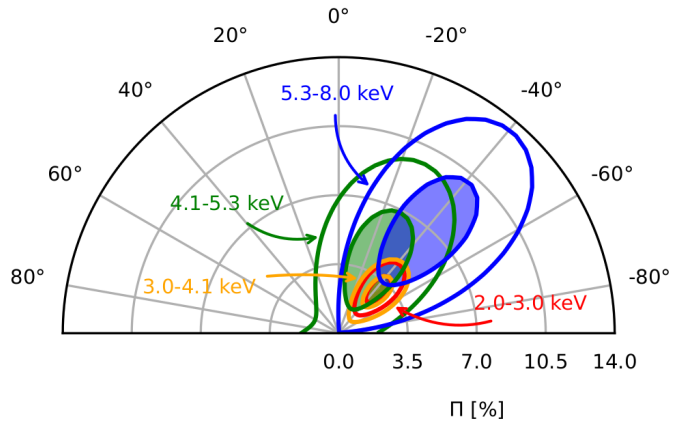


**Figure 5.** Polar plot of the polarization measured in different energy ranges with the spectral best-fit model. The filled contours correspond to the 68% ( $1\sigma$ ) and the outer contours to the 99.9% confidence levels, respectively.

linked the absorption parameters for the different detectors to it.

In our preferred model, the black hole mass and inclination are initially fixed to the values from the dynamical measurements (Orosz et al. 2014). Because in the IXPE observation of Cyg X-1 the inclination of the innermost accretion disk from the X-ray spectroscopy and polarimetry was found to be different from the value for the orbital inclination (Krawczynski et al. 2022), we also performed an alternative spectral fit with free inclination. The best-fit value of the inclination changed slightly to  $i = 71.8^{+2.0}_{-1.2}$  deg, and corresponding inferred luminosity increased from  $L = 0.43 L_{\text{Edd}}$  to  $L = 0.48 L_{\text{Edd}}$ . The goodness of the fit improved by  $\Delta\chi^2 = 310 - 317 = -7$  compared to the initial fit. This improvement was only marginal and we conclude that the inclination of the accretion disk constrained from the X-ray spectra is consistent with the inclination of the binary system constrained from the optical measurements.

### 3.3. Spectro-polarimetric analysis

We first included the IXPE  $Q$  and  $U$  spectra into our analysis by taking our best-fitting spectral model from Table 2 and assigning a constant PD and PA to it using the `polconst` model. For  $Q$  and  $U$  spectra, we applied the same gain as for  $I$  spectra, and we also kept the cross-normalization factors. The only free parameters were the PD and PA, noted as  $A$  and  $\psi$  in the `polconst` model. Considering the full IXPE bandpass yields a PD of  $A = 3.2\% \pm 0.6\%$  and a PA  $\psi = -42^\circ \pm 6^\circ$ .

To investigate any energy dependence, we performed the fit in four different energy bands spanning 2–8 keV and calculated contours using 50 steps in each parameter. We defined the energy bands as: 2–3, 3–4.1, 4.1–5.3,

and 5.3–8 keV. Figure 5 shows the resulting contours in the polar plot of PD and PA. While there is an apparent trend of increasing PD with the energy as in Figure 2, the significance of the change is not high. The PD is consistent with being a constant below 5 keV, and increases with energy above 5 keV only at  $1\sigma$  confidence level.

We then proceeded to fit physical models that self-consistently predict energy-dependent polarization properties. Since no polarized slim-disk model currently exists, we were limited to fitting standard thin-disk models. We employed models from the relativistic package `KY` (Dovčiak et al. 2004), which has been developed for spectral, timing, and polarimetry analysis. We employed the relativistic thin Novikov-Thorne disk model `kynbrr` (Taverna et al. 2020). This includes the same parameters as `kerrbb`, with some extra parameters required to specify the polarization properties such as the position angle of the disk (and black hole) rotation axis on the plane of the sky  $\chi_0$ , the optical depth of electron scattering in the disk atmosphere  $\tau$ , and the albedo that defines the reflectivity of the disk surface for returning radiation (radiation that is lensed by a black hole such that it returns and reflects on the other part of the disk before reaching an observer). The `Stokes` parameter in the model allows us to define how the polarization is calculated. We used `Stokes` = 1 that reads the polarization from loaded  $I$ ,  $Q$ , and  $U$  spectra. The polarization characteristics of this model for various sets of accretion disk parameters and a more-detailed model description are presented in Mikusincova et al. (2023).

We also employed the absorbed `kynbrr` model using the spectral parameters from the fit with the `tbfeo × simpl*kerrbb` model. To avoid the fit being dominated by the total count spectrum, we fitted only  $Q$  and  $U$  spectra (i.e., without  $I$ ) with free  $\chi_0$  and additionally a free normalization of the model to account for differences between `kynbrr` and `kerrbb`. We obtained an acceptable fit with  $\chi^2/\nu = 28.4/28 \approx 1.0$  with  $\chi_0 = 47^\circ \pm 6^\circ$  and normalization parameter  $N_K = 0.066 \pm 0.013$ .<sup>5</sup>

#### 3.4. Black hole spin measurements from the polarimetry

For fitting the black-hole spin from the polarimetric measurements only, independently of the total spectrum, we employed the normalized  $Q/I$  and  $U/I$  spectra, to which we applied the `kynbrr` model with the

<sup>5</sup> `kynbrr` does not have distance as a model parameter. The normalization would be around 1 for the source at the distance of 10 kpc. The distance of LMC X-3 is  $\approx 50$  kpc and thus, the normalization value is expected to be around  $1/5^2 \approx 0.04$ , roughly consistent with the measurements.

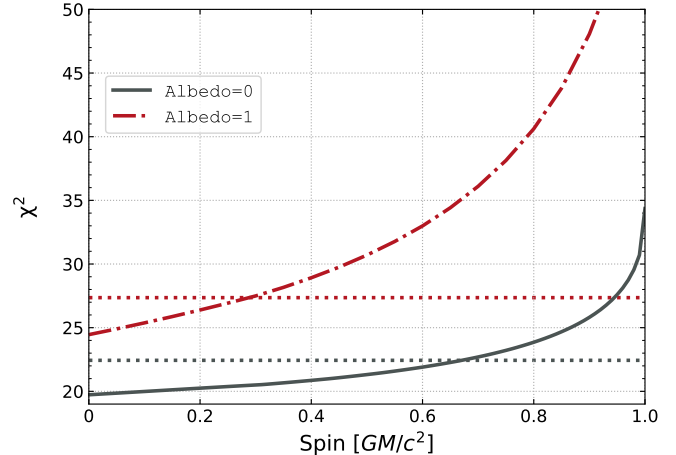


**Figure 6.** Polarimetry constraints of the black hole spin, expressed as goodness of the fit (as the  $\chi^2$  values) versus black-hole spin from  $Q/I$  and  $U/I$  fitting with the `kynbrr` model for two extreme values of albedo: 0 (black, solid line) and 1 (red, semi-dashed line). The dotted horizontal lines represent 90% confidence levels.

normalization fixed to 1. The `Stokes` parameter in the `kynbrr` model needs to be set to 8 for  $Q/I$  and 9 for  $U/I$ , respectively. We tested two cases of albedo, 0 and 1. While the albedo = 0 means that no returning radiation is taken into account, albedo = 1 corresponds to the 100% reflectivity of the gravitationally light-bended returning radiation. The albedo is important mainly for a highly spinning black-hole when the ISCO extends closer to the black hole and more returning radiation is expected (Cunningham 1976).

For the albedo equal to 0, we fitted the  $Q/I$  and  $U/I$  spectra with the black-hole spin  $a$  and  $\chi_0$  as free parameters. We obtained a perfectly acceptable fit with  $\chi^2/\nu = 19.9/20 \approx 1.0$ ,  $a < 0.66$  and  $\chi_0 = 44^\circ 6 \pm 6^\circ 4$ . For a non-zero value of the albedo, the model is currently calculated for 20 values of the spin and does not allow for a direct fitting of this parameter. We applied the `steppar` command in `XSPEC` to calculate the  $\chi^2$  values for the different values of the black-hole spin, and for the comparison, we performed the same procedure for albedo equal to 0.

Figure 6 shows the dependence of the fit goodness against the spin value for the two cases with albedo equal to 0 and 1, respectively. With the 90% confidence, the black-hole spin is required to be lower than 0.66 for albedo = 0 and lower than 0.3 for albedo = 1. The case of albedo = 0 is preferred by the fit with lower  $\chi^2$  values. The results indicate that the sole polarimetry measurements are consistent with the low black-hole spin in LMC X-3, independently of the spectral fitting.

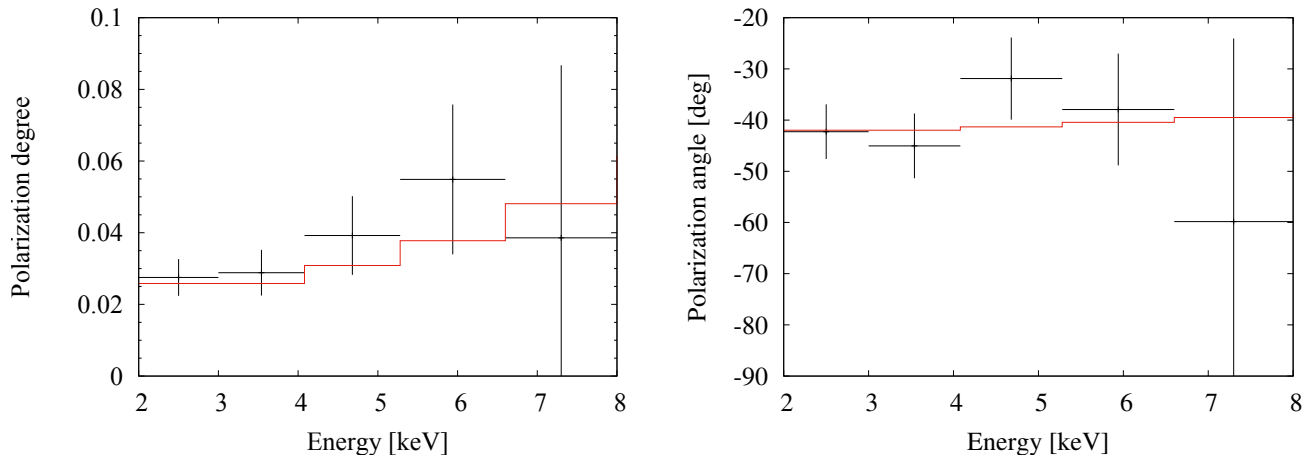


**Figure 7.** PD (*left*) and PA (*right*) fitted by the `kynbbrr` model with the optical depth  $\tau = 4.5$ .

#### 4. DISCUSSION AND CONCLUSIONS

With the best-fit spectral model, we obtained for the polarimetry:  $PD = 3.2\% \pm 0.6\%$  and  $PA = -42^\circ \pm 6^\circ$  in the 2–8 keV energy band, assuming a constant polarization over energy. These measurements are in perfect agreement with the values ( $PD = 3.1\% \pm 0.4\%$  and  $PA = -45^\circ \pm 4^\circ$ ) obtained from an alternative analysis using the `xpbin` tool within the `pcube` algorithm (see Section 3.1).

Regarding the PA measurements, there are no known large-scale physical structures associated with LMC X-3 with which to compare the PA. LMC X-3 is persistently in the high/soft state and no jet has been detected in the radio despite several efforts (Fender et al. 1998; Gallo et al. 2003; Lang et al. 2007). There is also no evidence for ionization cones in the far-UV (Hutchings et al. 2003), or presence of any significant emission or absorption lines in soft X-rays (Page et al. 2003).

The level of the PD is consistent with expectations for the thermal disk emission around a black hole with a low spin and high inclination (see the case of  $a = 0$  and  $i = 70^\circ$  in Figure 4 in Mikusincova et al. (2023) with a constant PD just slightly below 3%). The Novikov-Thorne model, assumed in the `kynbbrr` spectral model, provides a perfect fit to the X-ray polarimetry despite the best-fit spectral model employing a slim disk. This is most likely explained by the limited statistics of the X-ray polarimetry fit, while the spectral fit is sensitive to small differences between the `kerrbb` and `slimbb` models, which can possibly be attributed to the treatment of the spectral hardening in these models.

The black-hole spin, solely constrained from the X-ray polarimetry using normalized Stokes parameters  $Q/I$  and  $U/I$ , is consistent with the results of determining the spin from spectral fitting. The constraints on the spin are tighter if the reflection of the returning radi-

ation is taken into account, but even for a model with no reflected returning radiation (albedo=0), the spin is constrained to be less than 0.7 (see Figure 6).

While the X-ray polarization is well described by the model with constant PD with energy, the data tentatively indicate an increase of the PD with energy, which is most prominently visible in the plot showing the results from the `pcube` analysis (see Figure 2, especially above 5 keV). At higher energies, however, the uncertainty of the polarization measurements increases due to a lower number of counts and thus in our case, the PD increase with energy is suggested with only marginal statistical significance (see Figure 5).

The increasing energy dependence is included in the model variant `kynbbrr` of the KY package. We employed this model using the same spectral parameters from the fit of the `simpl*kerrbb` model, and we fitted only  $Q$  and  $U$  spectra. The parameter  $\tau$  was a free parameter together with  $\chi_0$  and the normalization of the model. We fixed the albedo to 0, and we obtained a very good fit with  $\chi^2/\nu = 26.5/27 \approx 1.0$ . The best-fit parameters are  $\chi_0 = 47^\circ \pm 6^\circ$ ,  $\tau = 4.5^{+4.5}_{-2.6}$ , and  $N_K = 0.04 \pm 0.02$ . The PD and PA using this model are shown in Figure 7. However, compared to results obtained with `kynbbrr` (see Section 3.3, with  $\chi^2/\nu = 28.4/28$ ), the improvement is not statistically significant.

The trend of increasing PD with energy and roughly constant PA seem, nevertheless, to be typical for observations of BHXRBs in the high/soft state. A comparison of the behavior of the PD with energy for three BHXRBs in the high/soft state is shown in Figure 8, where a similar trend is apparent for all sources. Various explanations have been proposed, and different scenarios might be responsible for the observed trend in different sources. In the most prominent case of 4U 1630–47,

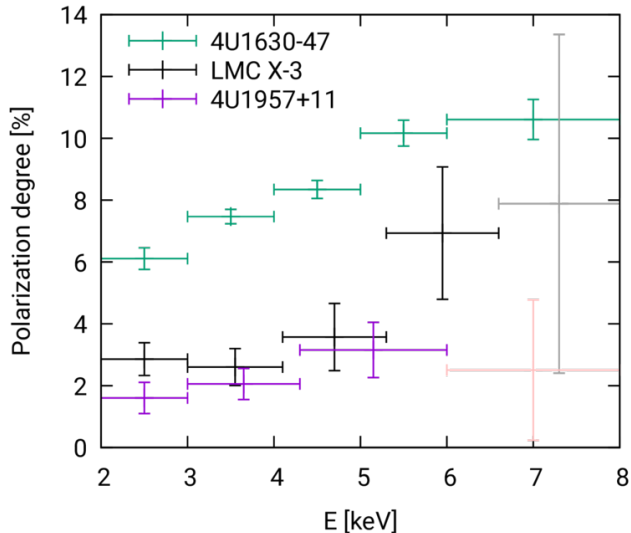


**Figure 8.** Comparison of the energy dependence of the PD in X-ray binaries in the high/soft state dominated by the thermal emission of the accretion disk.

the PD increase with energy is statistically very significant. A possible explanation attributes this to absorption in the upper layer of the accretion disk in combination with a relativistic bulk motion, which could also explain a higher PD than expected from an accretion disk with the electron scattering dominated atmosphere (Ratheesh et al. 2023). For 4U 1957+11, the increase can be explained by a combination of a high spin value and high albedo (Marra et al., in prep.). High albedo is, however, unlikely in the case of LMC X-3 given the low value of the black-hole spin. To perform a robust statistical test of the significance of the PD’s increase with energy, a longer observation would be needed to obtain a significant measurement up to 8 keV.

## 5. SUMMARY

We report on the first X-ray polarimetric observation of the accreting stellar-mass black hole LMC X-3 with the IXPE. The polarization is significantly detected with the PD being  $3.2\% \pm 0.6\%$  and PA measured as  $-42^\circ \pm 6^\circ$  in the 2–8 keV energy band. We performed a spectropolarimetric fit including the accompanying observations by NICER, NuSTAR, and Swift satellites, showing

that the X-ray spectrum is best modeled by a slim accretion disk with the intrinsic luminosity  $L \approx 0.4 L_{\text{Edd}}$ . We used the spectral data to measure the black hole spin  $a \approx 0.2$ . Using solely the polarimetric normalized Stokes parameters  $Q/I$  and  $U/I$ , we obtained for the black-hole spin:  $a < 0.7$  at 90% confidence level, in agreement with the spectroscopic measurements.

## ACKNOWLEDGMENTS

The *Imaging X ray Polarimetry Explorer (IXPE)* is a joint US and Italian mission. The US contribution is supported by the National Aeronautics and Space Administration (NASA) and led and managed by its Marshall Space Flight Center (MSFC), with industry partner Ball Aerospace (contract NNM15AA18C). The Italian contribution is supported by the Italian Space Agency (Agenzia Spaziale Italiana, ASI) through contract ASI-OHBI-2017-12-I.0, agreements ASI-INAF-2017-12-H0 and ASI-INFN-2017.13-H0, and its Space Science Data Center (SSDC) with agreements ASI-INAF-2022-14-HH.0 and ASI-INFN 2021-43-HH.0, and by the Istituto Nazionale di Astrofisica (INAF) and the Istituto Nazionale di Fisica Nucleare (INFN) in Italy. This research used data products provided by the IXPE Team (MSFC, SSC, INAF, and INFN) and distributed with additional software tools by the High-Energy Astrophysics Science Archive Research Center (HEASARC), at NASA Goddard Space Flight Center (GSFC). This work made use of data supplied by the UK Swift Science Data Centre at the University of Leicester.

Jiří S., M.D., Jak.Pod., Mic.Bur. and V.K. thank GACR project 21-06825X for the support and institutional support from RVO:67985815. A.Y. and Mai.Bri. acknowledge the support from GAUK project No. 102323. A.I. acknowledges support from the Royal Society. A.V. thanks the Academy of Finland grant 355672 for support. P.-O.P. acknowledges financial support from the French Space Agency (CNES) and the French High Energy National Programme (PNHE) of CNRS. NRC, MRM, HK, KH, and SC acknowledge support by NASA grants 80NSSC22K1291, 80NSSC23K1041, and 80NSSC20K0329.

*Facilities:* IXPE, NICER, NuSTAR, Swift

## REFERENCES

- Arnaud, K. A. 1996, in ASP Conf. Ser., Vol. 101, Astronomical Data Analysis Software and Systems V, ed. G. H. Jacoby & J. Barnes (San Francisco: ASP), 17–20
- Baldini, L., Bucciantini, N., Lalla, N. D., et al. 2022, SoftwareX, 19, 101194, doi: [10.1016/j.softx.2022.101194](https://doi.org/10.1016/j.softx.2022.101194)

- Belloni, T. M. 2010, in *Lecture Notes in Physics*, Berlin Springer Verlag, ed. T. Belloni, Vol. 794, 53, doi: [10.1007/978-3-540-76937-8\\_3](https://doi.org/10.1007/978-3-540-76937-8_3)
- Bhuvana, G. R., Radhika, D., & Nandi, A. 2022, *Advances in Space Research*, 69, 483, doi: [10.1016/j.asr.2021.09.036](https://doi.org/10.1016/j.asr.2021.09.036)
- Blackburn, J. K. 1995, in *ASP Conf. Ser.*, Vol. 77, *Astronomical Data Analysis Software and Systems IV*, ed. R. A. Shaw, H. E. Payne, & J. J. E. Hayes (San Francisco: ASP), 367
- Burrows, D. N., Hill, J. E., Nousek, J. A., et al. 2005, *SSRv*, 120, 165, doi: [10.1007/s11214-005-5097-2](https://doi.org/10.1007/s11214-005-5097-2)
- Chandrasekhar, S. 1960, *Radiative Transfer* (New York: Dover Publications)
- Connors, P. A., Piran, T., & Stark, R. F. 1980, *ApJ*, 235, 224, doi: [10.1086/157627](https://doi.org/10.1086/157627)
- Connors, P. A., & Stark, R. F. 1977, *Nature*, 269, 128, doi: [10.1038/269128a0](https://doi.org/10.1038/269128a0)
- Cunningham, C. 1976, *ApJ*, 208, 534, doi: [10.1086/154636](https://doi.org/10.1086/154636)
- Done, C., Gierliński, M., & Kubota, A. 2007, *A&A Rv*, 15, 1, doi: [10.1007/s00159-007-0006-1](https://doi.org/10.1007/s00159-007-0006-1)
- Dovciak, M., Steiner, J. F., Krawczynski, H., & Svoboda, J. 2023, *The Astronomer's Telegram*, 16084, 1
- Dovciak, M., Karas, V., & Yaqoob, T. 2004, *ApJS*, 153, 205, doi: [10.1086/421115](https://doi.org/10.1086/421115)
- Dovciak, M., Muleri, F., Goosmann, R. W., Karas, V., & Matt, G. 2008, *MNRAS*, 391, 32, doi: [10.1111/j.1365-2966.2008.13872.x](https://doi.org/10.1111/j.1365-2966.2008.13872.x)
- Ebisawa, K., Makino, F., Mitsuda, K., et al. 1993, *ApJ*, 403, 684, doi: [10.1086/172239](https://doi.org/10.1086/172239)
- Evans, P. A., Beardmore, A. P., Page, K. L., et al. 2009, *MNRAS*, 397, 1177, doi: [10.1111/j.1365-2966.2009.14913.x](https://doi.org/10.1111/j.1365-2966.2009.14913.x)
- Fender, R. P., Southwell, K., & Tzioumis, A. K. 1998, *MNRAS*, 298, 692, doi: [10.1046/j.1365-8711.1998.01680.x](https://doi.org/10.1046/j.1365-8711.1998.01680.x)
- Frank, J., King, A., & Raine, D. J. 2002, *Accretion Power in Astrophysics: Third Edition*
- Gallo, E., Fender, R. P., & Pooley, G. G. 2003, *MNRAS*, 344, 60, doi: [10.1046/j.1365-8711.2003.06791.x](https://doi.org/10.1046/j.1365-8711.2003.06791.x)
- Gehrels, N., Chincarini, G., Giommi, P., et al. 2004, *ApJ*, 611, 1005, doi: [10.1086/422091](https://doi.org/10.1086/422091)
- Gendreau, K. C., Arzoumanian, Z., & Okajima, T. 2012, in *Proc. SPIE*, Vol. 8443, *Space Telescopes and Instrumentation 2012: Ultraviolet to Gamma Ray*, ed. T. Takahashi, S. S. Murray, & J.-W. A. den Herder, 844313, doi: [10.1117/12.926396](https://doi.org/10.1117/12.926396)
- Gierliński, M., & Done, C. 2004, *MNRAS*, 347, 885, doi: [10.1111/j.1365-2966.2004.07266.x](https://doi.org/10.1111/j.1365-2966.2004.07266.x)
- Harrison, F. A., Craig, W. W., Christensen, F. E., et al. 2013, *ApJ*, 770, 103, doi: [10.1088/0004-637X/770/2/103](https://doi.org/10.1088/0004-637X/770/2/103)
- HI4PI Collaboration, Ben Bekhti, N., Flöer, L., et al. 2016, *A&A*, 594, A116, doi: [10.1051/0004-6361/201629178](https://doi.org/10.1051/0004-6361/201629178)
- Hubeny, I., & Lanz, T. 1995, *ApJ*, 439, 875, doi: [10.1086/175226](https://doi.org/10.1086/175226)
- Hutchings, J. B., Winter, K., Cowley, A. P., Schmidtke, P. C., & Crampton, D. 2003, *AJ*, 126, 2368, doi: [10.1086/378606](https://doi.org/10.1086/378606)
- Kaastra, J. S., & Bleeker, J. A. M. 2016, *A&A*, 587, A151, doi: [10.1051/0004-6361/201527395](https://doi.org/10.1051/0004-6361/201527395)
- Krawczynski, H., Muleri, F., Dovciak, M., et al. 2022, *Science*, 378, 650, doi: [10.1126/science.add5399](https://doi.org/10.1126/science.add5399)
- Lang, C. C., Kaaret, P., Corbel, S., & Mercer, A. 2007, *ApJ*, 666, 79, doi: [10.1086/519553](https://doi.org/10.1086/519553)
- Leong, C., Kellogg, E., Gursky, H., Tananbaum, H., & Giacconi, R. 1971, *ApJL*, 170, L67, doi: [10.1086/180842](https://doi.org/10.1086/180842)
- Li, L.-X., Zimmerman, E. R., Narayan, R., & McClintock, J. E. 2005, *ApJS*, 157, 335, doi: [10.1086/428089](https://doi.org/10.1086/428089)
- McClintock, J. E., Narayan, R., & Steiner, J. F. 2014, *SSRv*, 183, 295, doi: [10.1007/s11214-013-0003-9](https://doi.org/10.1007/s11214-013-0003-9)
- Mikusincova, R., Dovciak, M., Bursa, M., et al. 2023, *MNRAS*, 519, 6138, doi: [10.1093/mnras/stad077](https://doi.org/10.1093/mnras/stad077)
- Mitsuda, K., Inoue, H., Koyama, K., et al. 1984, *PASJ*, 36, 741
- Novikov, I. D., & Thorne, K. S. 1973, in *Black Holes (Les Astres Occlus)* (New York: Gordon & Breach), 343–450
- Nowak, M. A., Wilms, J., Heindl, W. A., et al. 2001, *MNRAS*, 320, 316, doi: [10.1046/j.1365-8711.2001.03984.x](https://doi.org/10.1046/j.1365-8711.2001.03984.x)
- Orosz, J. A., Steiner, J. F., McClintock, J. E., et al. 2014, *ApJ*, 794, 154, doi: [10.1088/0004-637X/794/2/154](https://doi.org/10.1088/0004-637X/794/2/154)
- Page, M. J., Soria, R., Wu, K., et al. 2003, *MNRAS*, 345, 639, doi: [10.1046/j.1365-8711.2003.06967.x](https://doi.org/10.1046/j.1365-8711.2003.06967.x)
- Pietrzyński, G., Graczyk, D., Gallenne, A., et al. 2019, *Nature*, 567, 200, doi: [10.1038/s41586-019-0999-4](https://doi.org/10.1038/s41586-019-0999-4)
- Podgorny, J., Marra, L., Muleri, F., et al. 2023, *arXiv e-prints*, arXiv:2303.12034, doi: [10.48550/arXiv.2303.12034](https://doi.org/10.48550/arXiv.2303.12034)
- Poutanen, J., Veledina, A., & Beloborodov, A. M. 2023, *ApJL*, 949, L10, doi: [10.3847/2041-8213/acd33e](https://doi.org/10.3847/2041-8213/acd33e)
- Ratheesh, A., Dovciak, M., Krawczynski, H., et al. 2023, *arXiv e-prints*, arXiv:2304.12752, doi: [10.48550/arXiv.2304.12752](https://doi.org/10.48550/arXiv.2304.12752)
- Rees, M. J. 1975, *MNRAS*, 171, 457, doi: [10.1093/mnras/171.3.457](https://doi.org/10.1093/mnras/171.3.457)
- Remillard, R. A., Loewenstein, M., Steiner, J. F., et al. 2022, *AJ*, 163, 130, doi: [10.3847/1538-3881/ac4ae6](https://doi.org/10.3847/1538-3881/ac4ae6)
- Rodriguez Caverro, N., Marra, L., Krawczynski, H., et al. 2023, *arXiv e-prints*, arXiv:2305.10630, doi: [10.48550/arXiv.2305.10630](https://doi.org/10.48550/arXiv.2305.10630)
- Schnittman, J. D., & Krolik, J. H. 2009, *ApJ*, 701, 1175, doi: [10.1088/0004-637X/701/2/1175](https://doi.org/10.1088/0004-637X/701/2/1175)

- Shafee, R., McClintock, J. E., Narayan, R., et al. 2006, ApJL, 636, L113, doi: [10.1086/498938](https://doi.org/10.1086/498938)
- Shakura, N. I., & Sunyaev, R. A. 1973, A&A, 500, 33
- Sądowski, A., Abramowicz, M., Bursa, M., et al. 2011, A&A, 527, A17, doi: [10.1051/0004-6361/201015256](https://doi.org/10.1051/0004-6361/201015256)
- Smale, A. P., & Boyd, P. T. 2012, ApJ, 756, 146, doi: [10.1088/0004-637X/756/2/146](https://doi.org/10.1088/0004-637X/756/2/146)
- Sobolev, V. V. 1963, A treatise on radiative transfer (Princeton: Van Nostrand)
- Soffitta, P., Baldini, L., Bellazzini, R., et al. 2021, AJ, 162, 208, doi: [10.3847/1538-3881/ac19b0](https://doi.org/10.3847/1538-3881/ac19b0)
- Steiner, J. F., McClintock, J. E., Orosz, J. A., et al. 2014, ApJL, 793, L29, doi: [10.1088/2041-8205/793/2/L29](https://doi.org/10.1088/2041-8205/793/2/L29)
- Steiner, J. F., McClintock, J. E., Remillard, R. A., et al. 2010, ApJL, 718, L117, doi: [10.1088/2041-8205/718/2/L117](https://doi.org/10.1088/2041-8205/718/2/L117)
- Steiner, J. F., Narayan, R., McClintock, J. E., & Ebisawa, K. 2009, PASP, 121, 1279, doi: [10.1086/648535](https://doi.org/10.1086/648535)
- Straub, O., Bursa, M., Sądowski, A., et al. 2011, A&A, 533, A67, doi: [10.1051/0004-6361/201117385](https://doi.org/10.1051/0004-6361/201117385)
- Sunyaev, R. A., & Titarchuk, L. G. 1980, A&A, 86, 121
- Taverna, R., Zhang, W., Dovčiak, M., et al. 2020, MNRAS, 493, 4960, doi: [10.1093/mnras/staa598](https://doi.org/10.1093/mnras/staa598)
- Torpin, T. J., Boyd, P. T., Smale, A. P., & Valencic, L. A. 2017, ApJ, 849, 32, doi: [10.3847/1538-4357/aa8f96](https://doi.org/10.3847/1538-4357/aa8f96)
- Treves, A., Belloni, T., Chiappetti, L., et al. 1988, ApJ, 325, 119, doi: [10.1086/165987](https://doi.org/10.1086/165987)
- Veledina, A., Muleri, F., Poutanen, J., et al. 2023, arXiv e-prints, arXiv:2303.01174, doi: [10.48550/arXiv.2303.01174](https://doi.org/10.48550/arXiv.2303.01174)
- Wang, J., Mastroserio, G., Kara, E., et al. 2021, ApJL, 910, L3, doi: [10.3847/2041-8213/abec79](https://doi.org/10.3847/2041-8213/abec79)
- Weisskopf, M. C., Elsner, R. F., & O'Dell, S. L. 2010, in Society of Photo-Optical Instrumentation Engineers (SPIE) Conference Series, Vol. 7732, Space Telescopes and Instrumentation 2010: Ultraviolet to Gamma Ray, ed. M. Arnaud, S. S. Murray, & T. Takahashi, 77320E, doi: [10.1117/12.857357](https://doi.org/10.1117/12.857357)
- Weisskopf, M. C., Soffitta, P., Baldini, L., et al. 2022, JATIS, 8, 026002, doi: [10.1117/1.JATIS.8.2.026002](https://doi.org/10.1117/1.JATIS.8.2.026002)
- Wilms, J., Allen, A., & McCray, R. 2000, ApJ, 542, 914, doi: [10.1086/317016](https://doi.org/10.1086/317016)
- Wilms, J., Nowak, M. A., Pottschmidt, K., et al. 2001, MNRAS, 320, 327, doi: [10.1046/j.1365-8711.2001.03983.x](https://doi.org/10.1046/j.1365-8711.2001.03983.x)
- Wu, K., Soria, R., Page, M. J., et al. 2001, A&A, 365, L267, doi: [10.1051/0004-6361:20000229](https://doi.org/10.1051/0004-6361:20000229)
- Yilmaz, A., Svoboda, J., Grinberg, V., et al. 2023, MNRAS, doi: [10.1093/mnras/stad2339](https://doi.org/10.1093/mnras/stad2339)
- Zdziarski, A. A., & Gierliński, M. 2004, Progr. Theor. Phys. Suppl., 155, 99, doi: [10.1143/PTPS.155.99](https://doi.org/10.1143/PTPS.155.99)